Micromachined Chip Scale Thermal Sensor for Thermal Imaging

Journal:	*ACS Nano*
Manuscript ID	nn-2017-08504x.R4
Manuscript Type:	Article
Date Submitted by the Author:	02-Feb-2018

Complete List of Authors:	Shekhawat, Gajendra; Northwestern University, Institute for Nanotechnology Ramachandran, Srinivasan; APPNANO Jiryaei Sharahi, Hossein; University of Calgary Schulich School of Engineering, Mechanical and Manufacturing Engineering Sarkar, Souravi; Northwestern University Hujsak, Karl; Northwestern University Li, Yuan; Northwestern University, Materials Science and Engineering Hagglund, Karl; Northwestern University Kim, Seonghwan; University of Calgary, Mechanical and Manufacturing Engineering Aden, Gary; APPNANO Chand, Ami; Applied NanoStructures, Inc. , Dravid, Vinayak; Northwestern University, Materials Science & Engineering

Micromachined Chip Scale Thermal Sensor for Thermal Imaging

Gajendra S. Shekhawat,[#*1] Srinivasan Ramachandran,[*2] Hossein Jiryaei Sharahi,[3] Souravi Sarkar,[1] Karl Hujsak,[1]Yuan Li,[1] Karl Hagglund,[1] Seonghwan Kim,[3] Gary Aden,[2] Ami Chand,[2#] and Vinayak P. Dravid,[1#]

[1] Department of Material Science and Engineering and NU*ANCE* Center, Northwestern University, Evanston, IL 60208

[2] APPNANO, 415 Clyde Ave., Mountain View, California 94043

[3] Department of Mechanical and Manufacturing Engineering, University of Calgary, AB, Canada.

Abstract

The lateral resolution of scanning thermal microscopy (SThM) has hitherto never approached that of mainstream atomic force microscopy, mainly due to poor performance of the thermal sensor. Herein, we report a nanomechanical system based thermal sensor (thermocouple) that enables high lateral spatial resolution that is often required in nanoscale thermal characterization in wide range of applications. This thermocouple-based probe technology delivers excellent lateral resolution (~ 20 nm),

extended high temperature measurements greater than 700°C without cantilever bending, and a very high thermal sensitivity (~0.04 °C). The origin of significantly improved figures-of-merit lies in the probe design that consists of a hollow silicon tip integrated with a vertically oriented thermocouple sensor at the apex (low thermal mass) which interacts with the sample through a metallic nanowire (50 nm diameter), thereby achieve high lateral resolution. The efficacy of this approach to SThM is demonstrated by imaging embedded metallic nanostructures in silica core shell, metal nanostructures coated with polymer films, and metal-polymer interconnect structures. The nanoscale pitch and extremely small thermal mass of the probe promise significant improvements over existing methods and wide range of applications including in semiconductor devices, biomedical imaging, and data storage.

KEYWORDS: Thermal Imaging, Nanomechanical thermal sensor, metallic nanostructures, temperature mapping, thermal conductivity mapping

Scanning thermal microscopy (SThM) is a variant of scanning probe microscopy (SPM) wherein a sharp tip integrated with a thermal sensor is raster scanned over a sample to obtain its topography and thermal properties simultaneously. SThM probes have been used in several applications, including surface temperature measurements, thermal conductivity, thermodynamic characterization, calorimetry, thermo-mechanical actuation and chemical imaging.[1-7] Several sensor schemes have been implemented for

SThM including, Schottky diode[8] and bimetallic cantilevers,[9] but majority of the work has been dominated by two types of thermal sensing elements: (i) thermocouple, (ii) thermistor. The first SThM was demonstrated using coaxial thermocouple formed at the end of a metal tip. Since then several configurations of thermocouple sensing elements have been reported.[10-13] Metal resistive heaters like Wollaston wire[14] or a micro fabricated wire encased in polyimide[15] were originally developed for thermo mechanical data storage,[16,17] but have since been used in many other applications that take advantage of their thermal stability.

SThM[18-20] has come a long way since its invention in 1992 and plays a leading role in the investigation of thermal properties on the nanoscale. However, the lateral resolution of SThM has never reached that of mainstream AFM methods, mainly due to the bulky structure of the sensor (>100 nm to microns). In the semiconductor industry, as the device operational length scales continues to decrease to the order of electron and phonon mean free paths (~50 nm), heat generation and dissipation become a critical factor in determining reliable performance. At these length scales, phonons play a dominant role in heat transport.[21]

Apart from semiconductor devices, other nanoscale devices such as optoelectronics, electromechanical actuators/sensors, thermoelectric materials, also face similar heat generation challenges. For example, nanotube-based electronics,[22,23] nanowire array-based lasers,[24,25] super lattices based thin film thermoelectric

materials[26,27] and nanowires.[28,29] The lack of thermal metrology at the nanoscale is a major impediment for scientific and economic developments.

There is a pressing need for a SThM that can correlate thermal properties with the structure at <100 nm. A lateral resolution in the range of 10-50 nm will immensely drive developments in several fields of research.

Efforts to increase resolution of scanning thermal microscopy made a progress recently with reported 10 nm resolution on crystalline samples and under high vacuum conditions.[30,31]. Recent report[30] have demonstrated 10 nm resolution on crystalline sample (InAs nano wire). However, this method has critical limitations, for example: i) it is applicable only to samples whose temperature could be modulated. This requires that the sample be electrically conductive thereby limiting its application to conductive samples, ii) the modulation frequency needs to be determined for each sample, iii) steady temperature sources cannot be characterized and finally, these probes are not available commercially. On the other hand, our method can be applied on all samples (crystalline/amorphous/conductive/dielectric) and the probes are available for the large scientific community. Other achievements[31] have reported similar resolution (~10 nm) and sensitivity (~15 mK) under ultra-high vacuum condition. The absence of water layer on the sample surface under vacuum makes this possible as the parasitic heat transfer between tip-sample through adsorbed water layer is eliminated and this improves resolution and sensitivity. Earlier developments[12,13] has made thermocouple probes for

SThM and data recording applications. The major challenge is controlling the thermocouple mass for faster thermal imaging applications. Secondly, the thermocouple is at the apex of the tip directly contacting the sample which limits the probe life and finally it doesn't allow AFM lever laser to use the probe in the active mode without an external power source.

In this paper, we demonstrate thermocouple based probe technology that delivers excellent spatial resolution (~ 20 nm) and high thermal sensitivity (~ 0.04 °C). This is made possible through an innovative probe design that consists of a hollow silicon tip integrated with vertically oriented thermocouple sensor at the apex which is connected to the sample by a metallic nanowire offering up to 20 nm lateral resolution. Also, the low mass of the sensor and low thermal resistance at the tip coupled with high thermal resistance elsewhere limits heat loss from the probe during measurement achieving accurate temperature measurements. The choice of thermocouple and cantilever materials enable extended temperature measurements up to 700°C or more without significant cantilever bending. The probe design also offers the convenience of using the AFM's optical lever laser to heat the thermocouple above room temperature to enable thermal conductivity mapping or temperature mapping, by appropriate positioning of the laser on the cantilever without the need for complex electronics and expensive current source to operate in active mode. Above all, the thermal probe is micro fabricated using scalable semiconductor processing techniques to ensure

reproducibility, a major advantage over growth-based methods of nanowires on an AFM probe.

RESULTS AND DISCUSSIONS

Bruker Dimension ICON systems were used with the thermal module to map high resolution thermal properties and topography simultaneously. Figure 1a shows

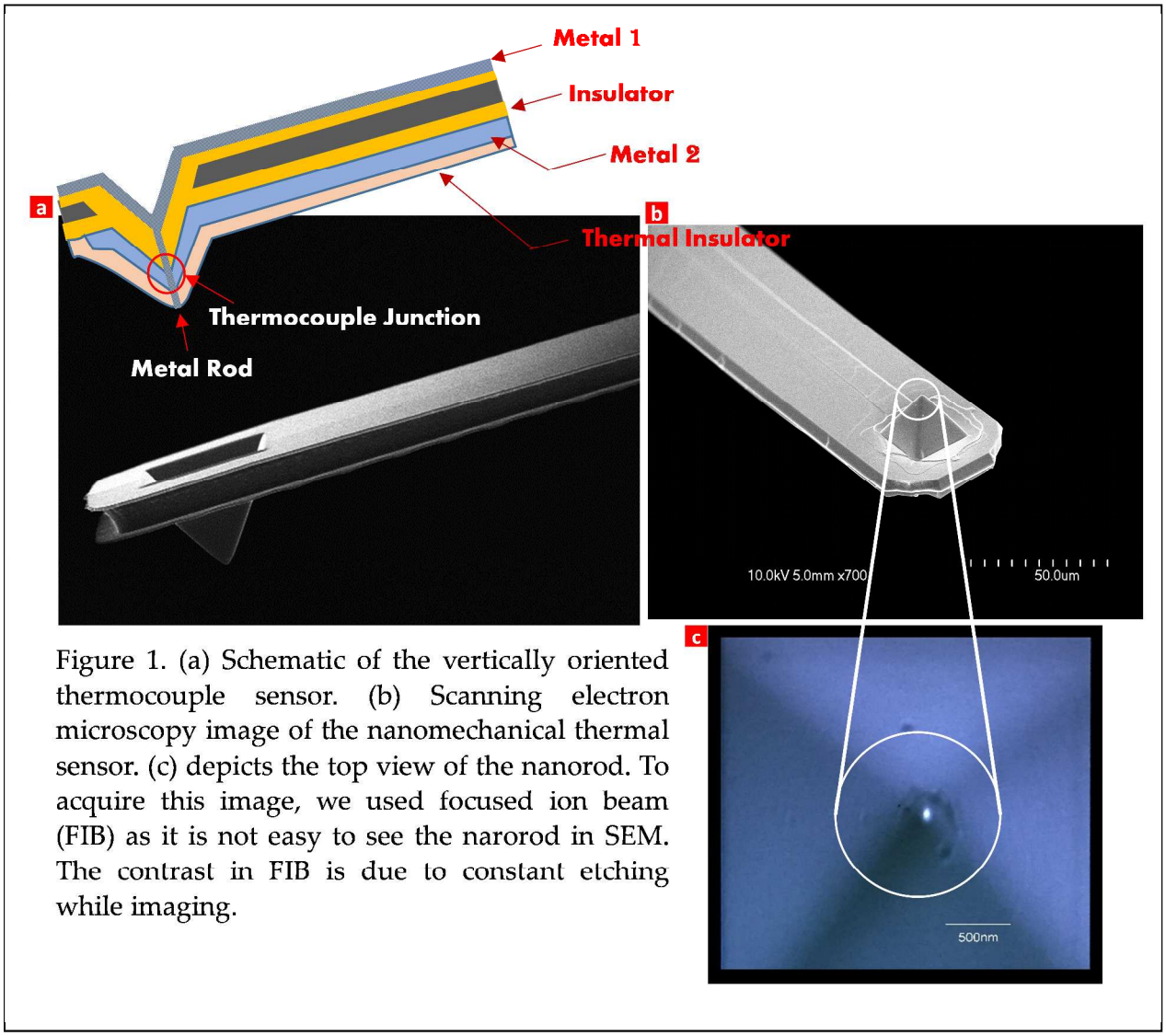

Figure 1. (a) Schematic of the vertically oriented thermocouple sensor. (b) Scanning electron microscopy image of the nanomechanical thermal sensor. (c) depicts the top view of the nanorod. To acquire this image, we used focused ion beam (FIB) as it is not easy to see the narorod in SEM. The contrast in FIB is due to constant etching while imaging.

the schematics and scanning electron microscopy image of thermal probe (Figure 1b). Figure 1c depicts the top view of the metal nanorod.

In conventional thin film thermocouple probes, the junction is a surface metal laying horizontally (side-side thus increasing the contact size of the sensor) and in direct contact with the sample. The size of the junction determines both the resolution and its life since the sensing element is directly exposed to the sample while scanning increases its wear. In our design, the junction is vertically oriented and connected to the sample by a thin nanowire-whose radius of curvature determines the lateral resolution and enhances sensitivity. The extended length of the nanowire (length beyond the thermocouple junction) helps to extend its operational life.

The thermal probe is nanofabricated using standard semiconductor and silicon micromachining technology. The basic tip material is chosen to be thermally and electrically insulating such as silicon dioxide or silicon nitride. After fabricating silicon tip of height about 10 μm to 15 μm, a local oxidation process is performed to oxidize the tip. The oxide thickness is kept about 1 μm. After the cantilever is defined and etched to a thickness of about 4μm, the silicon material from the tip is selectively etched to obtain a hollow tip. This hollow tip is made of silicon dioxide material. If required, the tip material can be chosen to be silicon nitride. The aperture in the tip is created by spin coating this photoresist such that tip apex is exposed. The oxide apex of the tip is then etched using dry etch process. The metal on the front is coated on the tip to define one of the thermocouple legs. The metal nanorod is formed before the backside metal is coated. The cantilever is made of single crystal silicon. The selection of materials of tip,

cantilever and thermocouple are primarily based on their thermal and electrical properties, to achieve high sensitivity of thermocouple sensor, high thermal resistance except at the nanowire to enhance sensitivity and accuracy; and minimize cantilever bending when measuring elevated temperatures. The tip is designed to direct heat transfer between thermocouple and the sample vertically into the junction through the metal nanowire encapsulated with a thermal insulator to minimize lateral heat flow from the sample to the nanowire or vice versa that enhances sensitivity and minimize topography related artifacts. More details on the probe structure and fabrication process are described in the patent as reference material.[32]

The probe can be operated in either temperature mapping mode (TMM) to measure surface temperature or conductivity mapping mode (CMM) to map relative thermal conductivity by adjusting the location of AFM laser on the cantilever (Fig S1). In the CMM mode, the laser is positioned in such a way that it partially spills into the hollow pyramid to heat the thermocouple at the same time has sufficient SUM signal to monitor deflection as feedback signal for engaging the surface. In this mode, the tip is at higher temperature (typically ~ 20 °C above ambient) compared to the sample and heat flow from tip to the sample is proportional to the local conductivity variations. Higher conductive regions would draw more heat and appear darker in the image and vice versa. In the TMM mode, the laser is positioned away from the pyramid to minimize heating the thermocouple. We have imaged a silicon micro heater sample in TMM

mode (Figure 2) that mapped point to point variations in the surface temperature. The sample is a 5x10 μm silicon with varying doses of ion implant. When a voltage is applied across the high implanted area, the central low implanted area heats up (joule heating). The temperature mapping image captures the point to point variations in surface temperature along with topography.

Figure 2. Surface temperature mapping of a silicon micro heater. *Left panel*: schematic of the silicon micro-heater showing different degrees of ion implanted areas. Gray is plain silicon, blue is low dose implant and pink is high dose implant overlying plain silicon and low dose areas. *Middle panel:* topography and *Right panel:* TMM image. The temperature image captures the point-to-point variations in the surface temperature due to joule heating at the center and diffusion of heat by the underlying silicon.

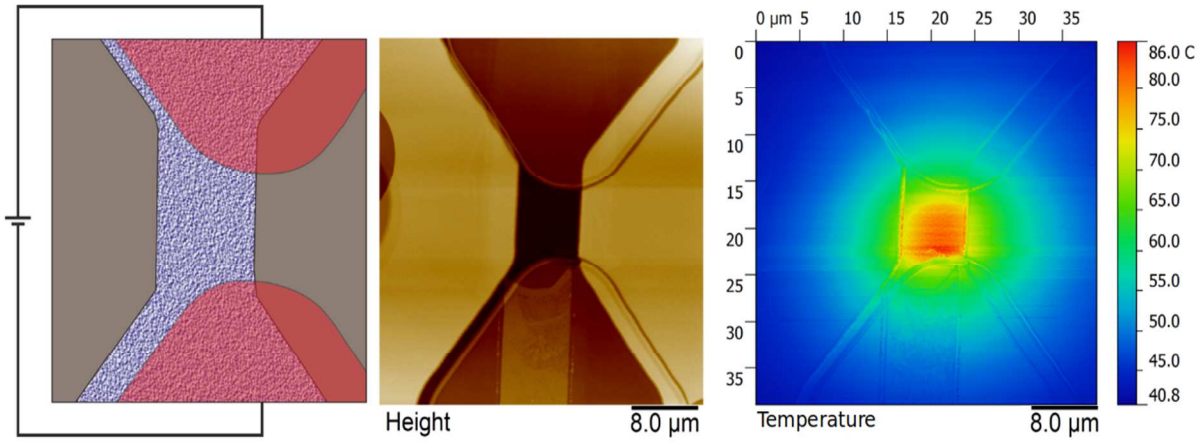

To demonstrate lateral resolution and depth sensitivity, a specimen consisting of gold nanoparticles (GNP, 40-50 nm in diameter) encapsulated in silica (approximately 200 nm in diameter) was bought from Sigma-Aldrich. The particles were dispersed on silicon dioxide substrate and imaged in conductivity contrast mode. Figure 3a shows the schematic of the thermal probe and silica particle interaction. AFM topography (Figure 3b) shows the distribution of well-dispersed silica spheres on the surface.

However, the thermal contrast (Figure 3c) originates from the differences in the thermal conductivities of gold nanoparticles, silica shell and the silicon dioxide substrate. Heat transfer from the probe to the sample changes the temperature of the probe while it scans the sample, thus allowing to map both thermal conductivity contrast and topography simultaneously.

Figure 3. (a) Schematic illustration of thermal probe interaction with gold nanoparticles (GNP) encapsulated in silica shell. (b) Shows AFM topography image. (C) Shows a remarkable thermal contrast from embedded GNP in silica. It clearly reveals a high thermal sensitivity, lateral resolution and contrast. The thermal image showing the difference in heat transfer from the tip to the silica shell and silicon dioxide substrate. (d) Shows the cross-sectional profile where temperature change (ΔT) from 0.8-0.9°C was recorded across the particle.

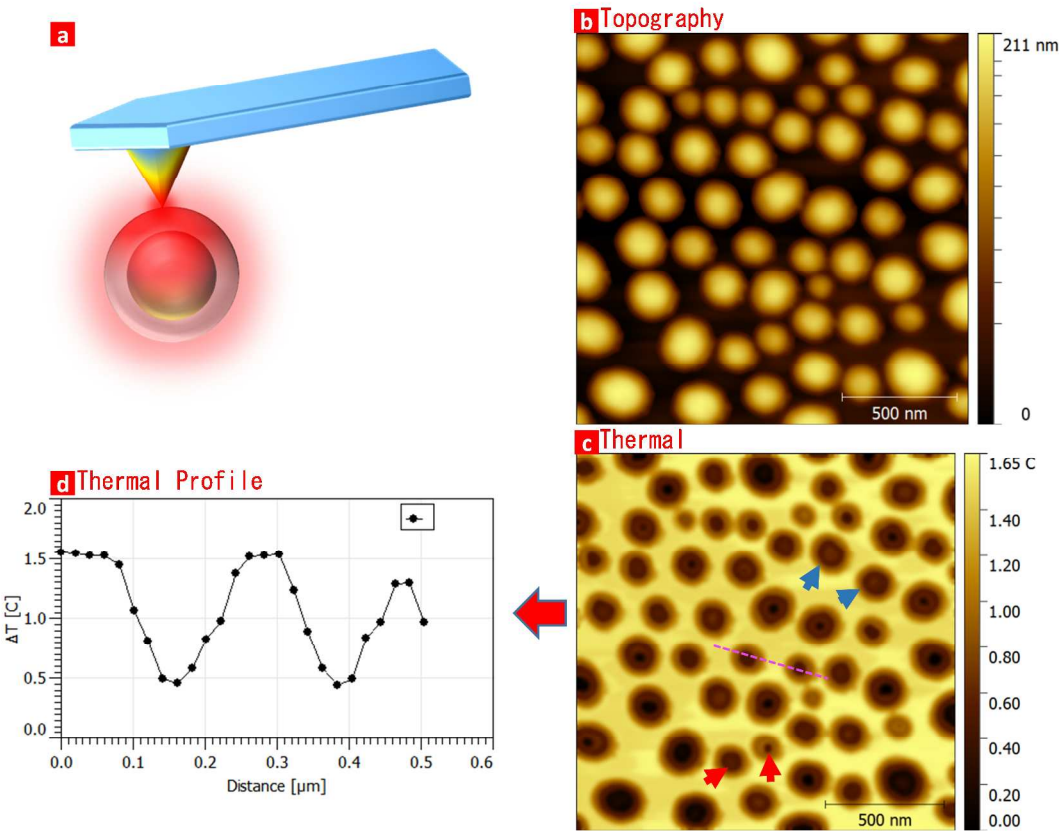

As gold is an excellent thermal conductor, more heat is drawn out from the tip to the embedded gold in silica where the coupling is very strong. AFM interprets low voltage (conducting material) as a darker color and higher voltage (thermally insulating material) as a lighter color. Figure 3d shows the temperature profile across the line (Figure 3c) and it clearly indicates that temperature change (ΔT) of 0.8-0.9°C is detected between the substrate and the GNP. This has potential applications in characterizing nano drug formulations, to study mixing and distribution of multicomponent polymers/composites based on thermal conductivity analysis.

Theoretical Study of Temperature Contrast Using Finite Elemental Analysis (FEA)

To validate the thermal contrast from embedded GNP in silica shell, we set up an axisymmetric finite element model of heat flow between the tip and nearby substrate using ANSYS R16.2 software. Figure 4 schematically shows the nano-composite model and their known values of mechanical and thermal properties applied in the simulation.

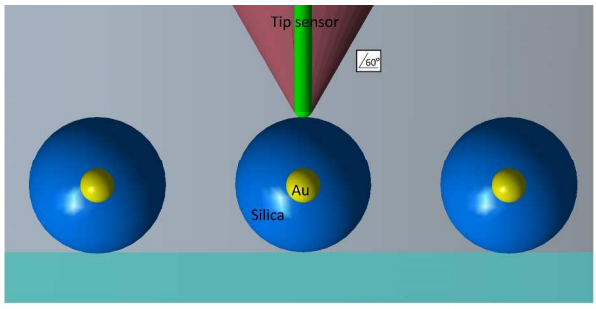

Figure 4. Schematic of the tip and the sample model. The gold nanoparticles were encapsulated in silica shell, and the SThM tip was modeled with a nanorod with a radius of 25 nm within a thermal insulator and it was extended with a straight line at an angle of 60°.

The model consists of 25 nm radius GNPs located within 100 nm radius. It is to be noted that prefect coupling

between GNPs and silica shell is assumed (Figure 4). Tip sensor temperature was experimentally measured when the cantilever was far away from the sample, and it was around 40°C when the AFM laser is positioned for CMM mode. Frictionless contact was assumed between air layer and tip sensor as well as the sample.

Four assumptions and approximations were considered in this theoretical approach: First, heat transfer from the tip to the environment by convection and thermal radiation are negligible.[33,34] Second, the experiment was performed in low humidity environment, so heat transfer through water meniscus formed near the contact area was relatively small. Third, the buried depth of nanoparticles was uniform. Fourth, the contact radius was assumed to be constant in all simulations.

Heat flow from a thermal probe influenced by several factors including contact area between tip-sample, the local thermal conductivity of the sample, and the temperature difference between probe and sample. The contact area between tip and sample was calculated using Hertzian contact theory.[35] For this, tip displacement was determined by a 200 nN load applied on the tip sensor and solved in incremental force of 1 nN. The simulation results showed the contact radius between the metal tip and silica-coated gold nanoparticles sample was around 10 nm.

Typical scan rate and number of the pixels per line in the experimental imaging was around 0.5 Hz and 512, respectively, that resulted in a dwell time of about 2

ms/pixel. This indicates that the locally heated volume in tip-sample reaches equilibrium in this time. Therefore, steady state heat transfer can be used for investigating heat flow from tip to sample with good approximation. In the thermal simulation, sample, and air boundaries were confined with ambient temperature at 22°C. Initially, all elements were automatically meshed, and further refinement was implemented at contact areas. The temperature variation between a buried nanoparticle and the matrix was then defined as:

$$\Delta T = T_m - T_{NP} \quad (1)$$

where T_m the temperature on a matrix is is surface without an underlying nanoparticle, and T_{NP} is the temperature on a matrix with an underlying GNP. The temperature of the contact area has been averaged in total elements that are involved in tip-sample contact. This area has been assumed to be constant in all simulations.

Based on the material properties of known materials and 1 mW laser power, the tip temperature was calculated as 43.81°C, when it was far away from the sample and surrounded with ambient air at 22°C. In this model and subsequent simulations, we used the same geometries, but with the properties of the elements set equal to the desired one. When the tip touched the sample (Figure S2), additional solid-solid conduction was added to air conduction. For a homogenous silica without the gold nanoparticle, the contact temperature decreased to 41.96°C. As expected, 1.85°C

temperature variation in contact area occurred because of the high thermal conductivity of silica than air. Moreover, when the tip touches the silica surface embedded with GNP, which is centrally encapsulated in silica shell with 100 nm radius, the contact temperature decreased to 40.72°C. This significant change in contact temperature, indicates that the gold nanoparticle draws more heat from the tip sensor due to its high thermal conductivity. $\Delta T = 41.96℃ - 40.72℃ = 1.24℃$, is well within the sensitivity of the probe.

To gain additional insights into the influence of GNP on the temperature distribution, the temperature profile was simulated along the direction perpendicular to the sample surface. This simulation was done for the same geometry that was depicted earlier (Figure S2). The temperature inside (Figure 5) the homogeneous silica sample (black circle) decreased exponentially till approached to the room temperature (22°C). However, for silica-coated GNP (red triangle), the temperature gradient across the GNP is almost constant due to its higher thermal conductivity.

Figure 5. Temperature profile inside the homogenous silica sample without gold nanoparticle (black circles) and silica coated gold nanoparticle (red triangles).

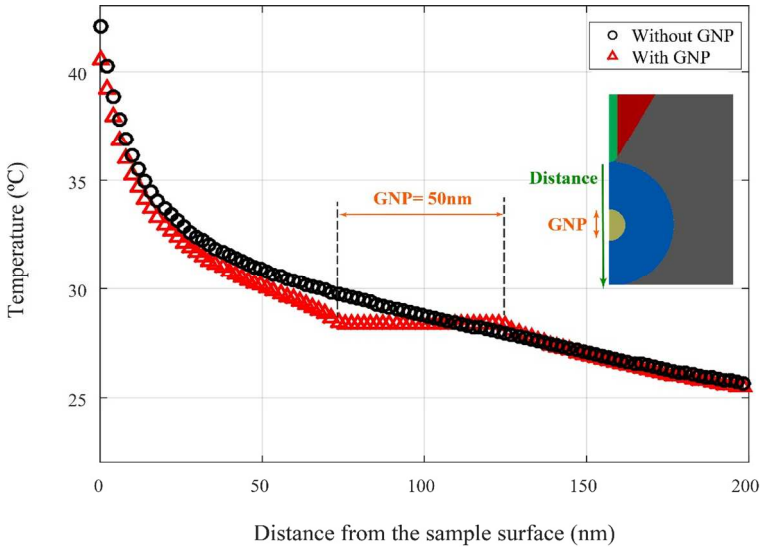

Additionally, temperature contrast as a function of nanoparticle depth was simulated using FEA. For this purpose, GNP with 25 nm radius was embedded in

Figure 6: (a) The temperature contrast (Equation 1) as a function of gold nanoparticle depth that is determined from FEA simulations. The FEA simulations have a gold nanoparticle, with a radius of 25 nm, embedded in a SiO_2 matrix. (b) The temperature contrast (Eq.1) as a function of the nanoparticle thermal conductivity. The carbon nanotube (CNT), diamond, silver (Ag), gold (Au), Aluminium (Al), Molybdenum (Mo), and steel nanoparticles have the same radius of 25 nm which are encapsulated in silica shell with 100 nm radius.

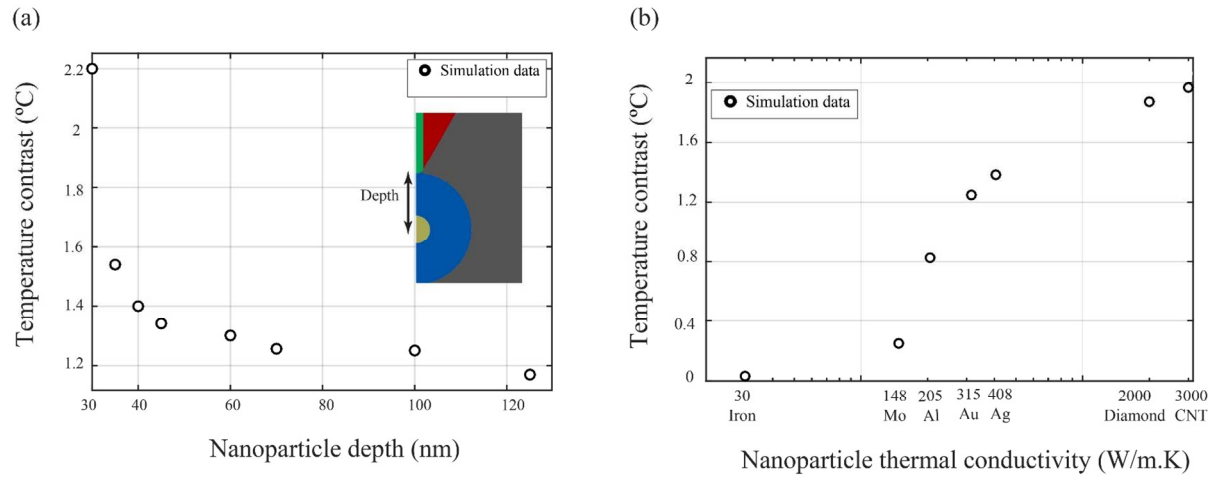

different depths of silica matrix. The temperature contrast (Figure 6a) reduced exponentially as the nanoparticle was buried further away from the sample surface. Lastly, to see the influence of thermal conductivity on the temperature contrast, the GNP has been substituted with other NPs with the same geometries. Carbon nanotube (CNT), diamond, silver (Ag), gold (Au), aluminum (Al), molybdenum (Mo), and steel nanoparticles that have the same radius of 25 nm are encapsulated in silica with 100 nm radius. The temperature contrast increases (Figure 6b) as the thermal conductivity of

buried NP increases. It confirmed that a gold nanoparticle with the same dimensions at the same depth is expected to be much easier to image than Iron.

Further to demonstrate the efficacy of high spatial thermal resolution, we fabricated an array of palladium (Pd) nanoparticles using focused ion beam lithography into an array followed by spin coating of a thin layer photoresist (around 50 nm). Topography scan (Figure 7a) shows polymer coating on these nanoparticles with some impressions of nanoparticles visible in the background since the thickness is very small. Corresponding thermal image (Figure 7b) reveals the thermal contrast from palladium nanoparticles embedded within the polymer. The sharp contrast in the thermal image indicates the high thermal conductivity of these nanoparticles, where the dark contrast on these particles is due to heat dissipation from the thermal probe to the Pd particles. The data presented here clearly demonstrates a lateral thermal resolution of around 20 nm. The temperature (ΔT) profile (Figure 7c) shows temperature variation of around 0.5-0.7°C was detected across the patterned array of Pd particles.

We further demonstrated the thermal resolution of this technology by patterning alternate lines of silver and copper using conventional optical photolithography. Both metals are ideally suitable for such experiments since they have almost similar thermal conductivity in pure metal form. Silver is susceptible to get oxidized easily in air; we, therefore, cleaned the samples in oxygen plasma and kept in a desiccator to avoid any further oxidation. The samples were transferred from desiccator to AFM system

chamber which was kept under vacuum (10^{-4} torr) to minimize oxidation during thermal scanning. JEOL SPM 5200 was used for these measurements. The topography of these patterned metal lines (Figure 8a) shows dots coated with thin layer of photoresist. Thermal conductivity image (Figure 8b) demonstrates the sensitivity of this probe to detect even a small variations in thermal conductivity (Cu-385 vs Ag-408 W/m.K).

Figure 7. (a) Typical AFM topography image is showing the polymeric coating with impressions of buried Pd nanoparticles. (b) The thermal contrast from the Pd nanoparticles buried in polymer coating demonstrating resolution down to ~20 nm and temperature variation of 0.5-0.7°C. (c) Temperature change (ΔT) profile across the patterned dots.

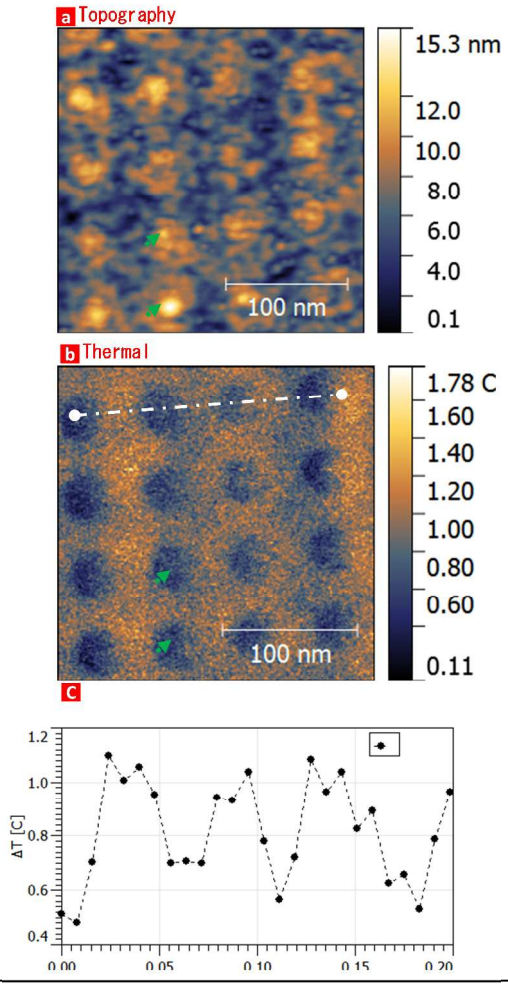

The darker color of silver is due to its higher thermal conductivity than copper. The RMS temperature variation between copper and silver was found to be 0.04°C, and it demonstrates the very high-temperature sensitivity of this thermal probe. Figure 8c shows the cross-sectional profile of the thermal contrast. While measuring the surface roughness, we have not considered the edge effects across the metal lines which usually happens

when probe is moving across the sharp step. To demonstrate that our probe design can be used for extended measurements without significant bending of the cantilever, we used an external modulated laser source to heat the thermocouple up to 760°C (Figure S3). The thermal data showed linear behavior throughout the temperature range and was symmetrical going up and down from room temperature (23°C) up to 760°C. It shows this technology have complete thermal isolation to the surroundings, thus

FIGURE 8: (a) Typical AFM topography image showing the alternate silver and copper lines. (b) The thermal contrast from both silver and copper lines demonstrating resolution down to 0.04°c. (c) temperature change (Δt) profile across the patterned lines. The RMS temperature variation between copper and silver was found to be 0.04 °c.

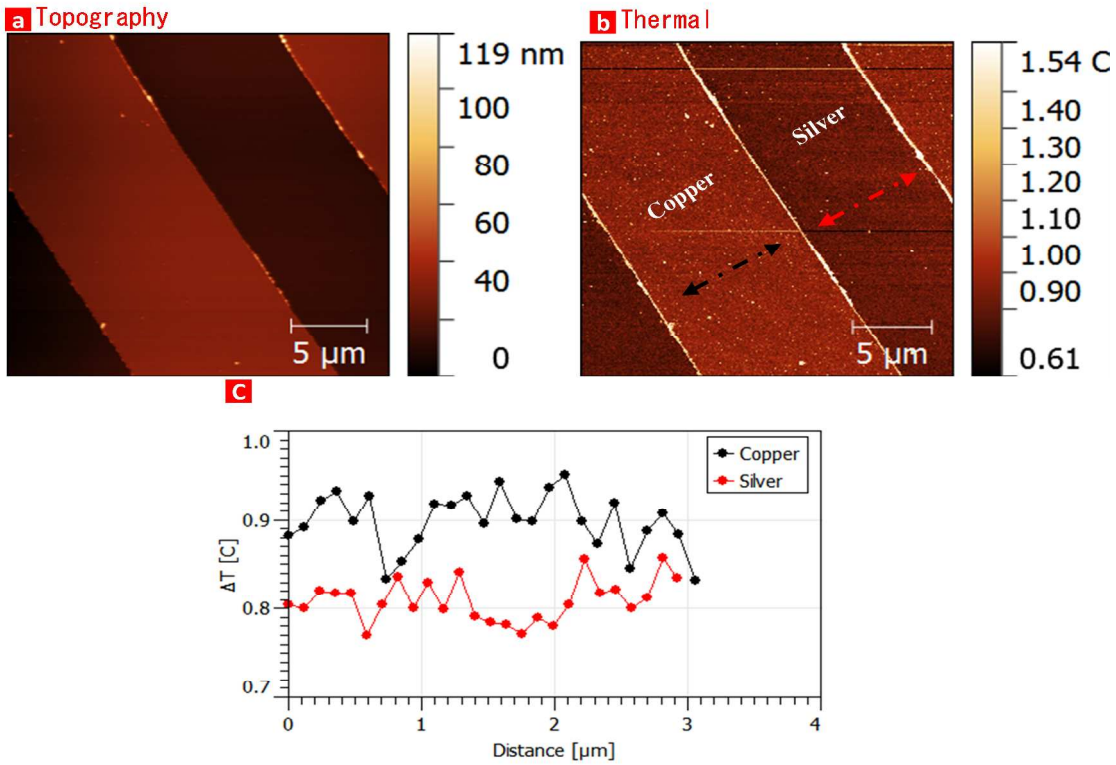

opening wide range of applications in studying the transition temperatures of materials and thermo mechanical analysis at nanoscale.

CONCLUSIONS

In conclusion, we have successfully designed and developed chip scale thermal probe with integrated thermocouple that achieved high lateral resolution (~20 nm), excellent thermal sensitivity (~0.04 °C) and high temperature measurements up to 760 °C. The probe design permits switching between temperature mapping and conductivity mapping modes just by appropriate positioning of AFM optical lever laser without the need for precision current source. The representative examples and applications modeled across different applications and materials demonstrate it as a versatile toolset for high-resolution thermal imaging for a wide range of materials and interfaces. We believe that the presented results fill the critical gap in the thermal spatial resolution at the ~20 nm scale with a wide range of applications in physical sciences, engineered systems and biology.

MATERIALS AND METHODS

The thermal imaging system could be interfaced with most AFM systems. The thermal module consists of a thermal probe, an interface box (pre-amplifier), an imaging amplifier and a controller. The voltage signal from the thermal probe is routed through the pre-amplifier to the imaging amplifier. The amplified thermal signal was input to the AFM controller for rendering thermal measurements using the AFM software (Figure S4). The imaging amplifier is an ultra-low noise amplifier (1 nV @ 1 KHz bandwidth) capable of up to 10,000x gain. The probes have a nominal thermal

sensitivity of about 9.34μV/°C, and more details about calibration procedure can be found in supplementary section.

To rule out thermal contrast arising from other factors like variations in laser intensity/environmental changes, we used a clean silicon wafer as a control to check for any variations in temperature across the surface Figure S5 shows a uniform surface temperature with variation around 0.02°C. The thermal profile clearly indicates negligible effect from other variables in the thermal contrast.

Note: * Gajendra Shekhawat & S. Ramachandran made equal contributions

AUTHOR INFORMATION

Corresponding Authors

#g-shekhawat@northwestern.edu, ami@appnano.com, v-dravid@northwestern.edu

ORCID

Gajendra Shekhawat: 0000-0003-3497-288X

Vinayak Dravid" 0000-0002-6007-3063

NOTES

The authors declare no competing financial interest

ACKNOWLEDGEMENTS

This work made use of the SPID facilities of the NU*ANCE* Center at Northwestern University which has received support from Soft and Hybrid Nanotechnology Experimental (SH_yNE) Resource (NSF-ECCS-1542205), MRSEC program (NSF DMR-1121262) at the Materials Research Center; the International Institute for Nanotechnology (IIN); the Keck Foundation; and the State of Illinois, through the IIN. This work was supported by grants from the National Science Foundation Award Number 1256188, IDBR: Development of Higher Eigen mode Ultrasound Bioprobe for Sub-Cellular Biological Imaging. We thankfully acknowledge NSF SBIR grant (1256640) awarded to APP*NANO* for the development of VertiSense SThM technology. S.K. would like to acknowledge the support from Canada Research Chairs (CRC) program and the Natural Sciences and Engineering Research Council of Canada (NSERC).

REFERENCES:

1. Kim, P.; Shi, L.; Majumdar, A.; McEuen, P. L., Thermal Transport Measurements of Individual Multiwalled Nanotubes. *Phys. Rev. Lett*. 2001, *87*, 215502
2. Shi, L.; Plyasunov, S.; Bachtold, A.; McEuen, P. L.; Majumdar, A., Scanning Thermal Microscopy of Carbon Nanotubes using Batch Fabricated Probes. *Appl. Phys. Lett.* 2000, *77*, 4295-4297.
3. Luo, K.; Shi, Z.; Varesi, J.; Majumdar, A., Sensor Nanofabrication, Performance, and Conduction Mechanisms in Scanning Thermal Microscopy. *J. Vac. Sci. Technol., B: Microelectron. Nanometer Struct.--Process., Meas., Phenom*. 1997, *15*, 349-360.
4. Hammiche, A.; Hourston, D. J.; Pollock, H. M.; Reading, M.; Song, M., Scanning Thermal Microscopy: Subsurface Imaging, Thermal Mapping of Polymer Blends, and Localized Calorimetry. *J. Vac. Sci. Technol., B: Microelectron. Nanometer Struct.--Process., Meas., Phenom*. 1996, *14*, 1486-1491.
5. Katzenmeyer, A. M.; Holland, G.; Chae, J.; Band, A.; Kjoller, K.; Centrone, A., Mid-Infrared Spectroscopy beyond the Diffraction Limit *Via* Direct Measurement of the Photothermal Effect. *Nanoscale* 2015, *7*, 17637-17641.

6. Jo, A.; Joo, W.; Jin, W.-H.; Nam, H.; Kim, J., Ultrahigh-Density Phase-Change Data Storage Without the use ff Heating. *Nat. Nanotechnol*. 2009, 4, 727-731.

7. Vattikuti, S. V. P.; Reddy, P. S.; Venkatesh, B., Probe-Based Data Storage Technology: Thermomechanical Storage –State of the Art. *Procedia Mater. Sci*. 2015, *10*, 419-432.

8. Leinhos, T.; Stopka, M.; Oesterschulze, E., Micromachined Fabrication ff Si Cantilevers with Schottky Diodes Integrated in the Tip. *Appl. Phys. A*. 1998, *66*, S65-S69.

9. Grover, R.; McCarthy, B.; Sarid, D.; Guven, I., Mapping Thermal Conductivity using Bimetallic Atomic Force Microscopy Probes. *Appl. Phys. Lett.* 2006, *88*, 233501.

10. Kim, K.; Chung, J.; Hwang, G.; Kwon, O.; Lee, J. S., Quantitative Measurement with Scanning Thermal Microscope by Preventing the Distortion due to the Heat Transfer Through the Air. ACS Nano 2011, *5*, 8700-8709.

11. Shi, L.; Plyasunov, S.; Bachtold, A.; McEuen, P. L.; Majumdar, A., Scanning Thermal Microscopy of Carbon Nanotubes using Batch Fabricated Probes. *Appl. Phys. Lett.* 2000, *77*, 4295-4297.

12. Lee, D. W.; Takahito, O.; Masayoshi, E., Fabrication of Thermal Microprobes with a Sub-100 nm Metal-to-Metal Junction. *Nanotechnol*. 2002, *13*, 29.

13. Dong-Weon, L.; Ono, T.; Abe, T.; Esashi, M., Microprobe Array with Electrical Interconnection for Thermal Imaging and Data Storage. *J. Microelectromech. Syst.* 2002, *11*, 215-221.

14. Pollock, H. M.; Hammiche, A., Micro-Thermal Analysis: Techniques and Applications. *J. Phys. D: Appl. Phys*. 2001, *34*, R23.

15. Tsukruk, V. V.; Gorbunov, V. V.; Fuchigami, N., Microthermal Analysis of Polymeric Materials. *Thermochim. Acta* 2002, *395*, 151-158.

16. Hyo-Jin, N.; Young-Sik, K.; Lee, C. S.; Won-Hyeog, J.; Seong Soo, J.; Il-Joo, C.; Jong-Uk, B., Integrated Nitride Cantilever Array with Si Heaters and Piezoelectric Detectors for Nano-Data-Storage Application. *IEEE Int. Conf. Micro Electro. Mech. Syst*., 18th , 2005. MEMS 2005, 247-250.

17. Lee, C. S.; Nam, H.; Kim, Y. S.; Jin, W. H.; Bu, J. U., PZT Cantilevers Integrated with Heaters and New Piezoelectric Sensors for SPM-Based Nano-Data Storage Application. *J. Korean Phys. Soc*. 2004, 45, 227-230.

18. Liang, X. M.; Sekar, P. K.; Zhao, G.; Zhou, X.; Shu, Z.; Huang, Z.; Ding, W.; Zhang, Q.; Gao, D., High Accuracy Thermal Conductivity Measurement of Aqueous Cryoprotective Agents and Semi-Rigid Biological Tissues Using a Microfabricated Thermal Sensor. *Sci. Rep*. 2015, *5*, 10377.

19. Shrestha, R.; Lee, K. M.; Chang, W. S.; Kim, D. S.; Rhee, G. H.; Choi, T. Y., Steady Heat Conduction-Based Thermal Conductivity Measurement of Single Walled Carbon Nanotubes Thin Film using a Micropipette Thermal Sensor. *Rev. Sci. Instrum*. 2013, *84*, 034901.

20. Nonnenmacher, M.; Wickramasinghe, H. K., Scanning Probe Microscopy of Thermal Conductivity and Subsurface Properties. *Appl. Phys. Lett*. 1992, 61, 168-170.

21. Pop, E.; Goodson, K. E., Thermal Phenomena in Nanoscale Transistors. *J. Electron. Packag* 2006, *128*, 102-108.

22. Chen, K.; Gao, W.; Emaminejad, S.; Kiriya, D.; Ota, H.; Nyein, H. Y. Y.; Takei, K.; Javey, A., Carbon Nanotubes: Printed Carbon Nanotube Electronics and Sensor Systems. *Adv. Mater.* 2016, *28*, 4396-4396.

23. Dmitriev, V.; Gomes, F.; Nascimento, C., Nanoelectronic Devices Based on Carbon Nanotubes. *J. Aerosp. Technol. Manage*. 2015, *7*, 53-62.

24. Sunayna, B. B.; Mohammad, S.; Muhammad, M.; Fan, G.; Jianlin, L., An Sb-Doped p-type Zno Nanowire based Random Laser Diode. *Nanotechnol.* 2016, *27*, 065204.

25. Shi, R.; Huang, C.; Zhang, L.; Amini, A.; Liu, K.; Shi, Y.; Bao, S.; Wang, N.; Cheng, C., Three Dimensional Sculpturing of Vertical Nanowire Arrays by Conventional Photolithography. *Sci. Rep.* 2016, *6*, 18886.

26. Chowdhury, I.; Prasher, R.; Lofgreen, K.; Chrysler, G.; Narasimhan, S.; Mahajan, R.; Koester, D.; Alley, R.; Venkatasubramanian, R., On-Chip Cooling by Superlattice-Based Thin-Film Thermoelectrics. *Nat. Nanotechnol.* 2009, *4*, 235.

27. Alexandrov, B.; Sullivan, O.; Kumar, S.; Mukhopadhyay, S. , Prospects of Active Cooling with Integrated Super-Lattice Based Thin-Film Thermoelectric Devices for Mitigating Hotspot Challenges in Microprocessors. *Asia and South Pacific Design Automation Conf. (APS-DAC)* 2012, 17th , 633-638.

28. Zhang, G.; Zhang, Q.; Bui, C.-T.; Lo, G.-Q.; Li, B., Thermoelectric Performance of Silicon Nanowires. *Appl. Phys. Lett.* 2009, *94*, 213108

29. Li, Y.; Buddharaju, K.; Singh, N.; Lee, S. J., Effect of Electrical Contact Resistance in a Silicon Nanowire Thermoelectric Cooler and a Design Guideline for on-Chip Cooling Applications. *J. Electron. Mater. 2013*, *42*, 1476-1481.

30. Menges, F.; Mensch, P.; Schmid, H.; Riel, H.; Stemmer, A.; Gotsmann, B., Temperature Mapping of Operating Nanoscale Devices By Scanning Probe Thermometry. *Nat. Commun.* 2016, *7*, 10874.

31. Kim, K.; Jeong, W.; Lee, W.; Reddy, P., Ultra-High Vacuum Scanning Thermal Microscopy for Nanometer Resolution Quantitative Thermometry. *ACS Nano* 2012, *6*, 4248-4257.

32. Goeckeritz, J.; Aden, G.; Chand, A., *U. S. Patent* 9,389,244,B2, 2016

33. Gomès, S.; Assy, A.; Chapuis, P.-O., Scanning Thermal Microscopy. *Phys. Status Solidi A* 2015, *212*, 477-494.

34. P. King, W.; Bhatia, B.; Felts, J.; Kim, H. J.; Kwon, B.; Lee, B.; Somnath, S.; Rosenberger, M., Heated Atomic Force Microscope Cantilevers and Their Applications. *Annu. Rev. Heat Transf*er 2013, 12, 287-326.

35. Johnson, K. L., Contact Mechanics. *Cambridge University Press*: Cambridge, 1987.

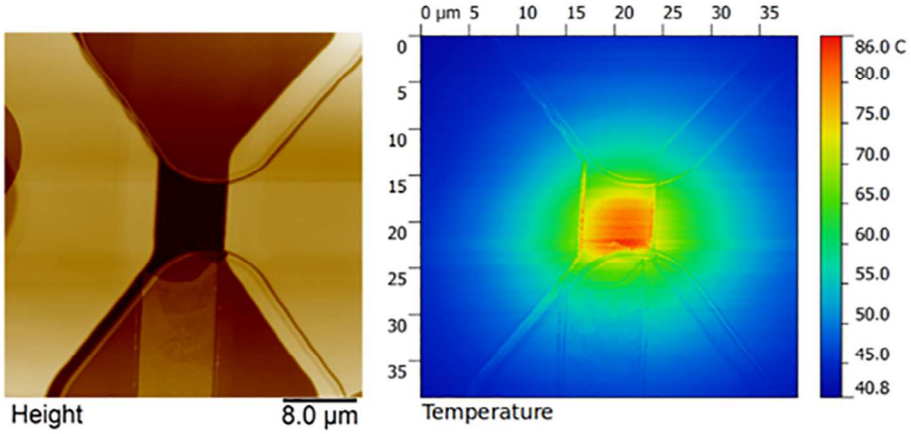

101x46mm (300 x 300 DPI)